

# High Schmidt number scalars in turbulence: Structure functions and Lagrangian theory

Michael S. Borgas

*CSIRO Atmospheric Research, PMB1 Aspendale, Victoria 3195, Australia*

Brian L. Sawford<sup>a)</sup>

*Department of Mechanical Engineering, Monash University, Clayton Campus, Wellington Road, Clayton, Victoria 3800, Australia*

Shuyi Xu, Diego A. Donzis, and P. K. Yeung

*School of Aerospace Engineering, Georgia Institute of Technology, Atlanta, Georgia 30332*

(Received 23 November 2003; accepted 15 June 2004; published online 20 September 2004)

We demonstrate the existence of Batchelor's viscous-convective subrange using direct numerical simulation (DNS) results to confirm the logarithmic dependence of the scalar structure function on the separation for the scalar field generated by stationary isotropic turbulence acting on a uniform mean scalar gradient. From these data we estimate the Batchelor constant  $\tilde{B}_\theta \approx 5$ . By integrating a piecewise continuous representation of the scalar variance spectrum we calculate the steady-state scalar variance as a function of Reynolds number and Schmidt number. Comparison with DNS results confirms the  $\text{Re}_\lambda^{-1}$  behavior predicted from the spectral integration, but with a coefficient about 60% too small. In the large Reynolds number limit the data give a value of 2.5 for the mechanical-to-scalar time scale ratio. The dependence of the data for the scalar variance on Schmidt number agrees very well with the spectral integration using the values of the Batchelor constant estimated from the structure function. We also carry out an exact Lagrangian analysis of the scalar variance and structure function, explicitly relating the Batchelor constant to the Lyapunov exponent for the separation of pairs of fluid particles within the turbulence dissipation subrange. Our results, particularly for the scalar variance, illustrate explicitly the singular nature of the zero diffusivity limit. For finite values of the Schmidt number and Reynolds number the viscous-convective subrange contribution to the variance can be significant even at moderate values of the Reynolds number. © 2004 American Institute of Physics. [DOI: 10.1063/1.1780550]

## I. INTRODUCTION

There has recently been much renewed interest<sup>1-9</sup> in the statistics of the scalar concentration in turbulence for high values of the Schmidt number  $\text{Sc} = \nu/\kappa$ , where  $\nu$  is the kinematic viscosity and  $\kappa$  is the scalar diffusivity. Partly this is due to the practical importance of the mixing processes associated with high Schmidt number scalars in turbulence in the ocean and in laboratory tracer studies.<sup>10-12</sup> It is also due to the conflicting experimental evidence for the existence of Batchelor's<sup>13</sup> classical  $k^{-1}$  viscous-convective subrange in the scalar spectrum<sup>14-17</sup> and the potential for direct numerical simulations to provide unambiguous confirmation of this  $k^{-1}$  scaling. Finally it is due to a fundamental interest in the influence of the small scale structure of the turbulence on the transport and distortion of a scalar trace material.<sup>9</sup> In this paper we revisit the classical results of Batchelor from both Eulerian and fully Lagrangian descriptions.

Written out fully, Batchelor's<sup>13</sup> result for the scalar variance spectrum in the viscous-convective subrange is

$$\phi(k) = \tilde{B}_\theta \chi (\nu/\varepsilon)^{1/2} k^{-1}, \quad \eta^{-1} \ll k \ll \eta_B^{-1}, \quad (1)$$

where  $\phi$  is the spectral density in a spherical shell of radius  $k$ ,  $k$  is the wave number magnitude,  $\chi$  is the rate of dissipation of scalar variance,  $\varepsilon$  is the rate of dissipation of turbulence kinetic energy, and the constant  $\tilde{B}_\theta$  is known as the Batchelor constant. The extent of the viscous-convective subrange is limited at large scales by the Kolmogorov length scale  $\eta = (\nu^3/\varepsilon)^{1/4}$  and at small scales by the Batchelor scale  $\eta_B = \eta \text{Sc}^{-1/2}$ . Batchelor's derivation was essentially Eulerian<sup>18</sup> although, the underlying idea involving an approximate treatment of the straining experienced by a small blob of scalar as it moves along its turbulent trajectory through the fluid, is Lagrangian. Subsequent treatments<sup>19,20</sup> improved on the approximation and various authors<sup>20-23</sup> have obtained the  $k^{-1}$  spectrum using two-point turbulence closure theories. Estimates for the Batchelor constant range from to 0.9<sup>20</sup> to 9.5<sup>2</sup>.

As noted by Batchelor,<sup>13</sup> Eq. (1) can be derived on dimensional grounds if the primary effect of convection on the fluctuating concentration  $\theta$  on scales smaller than the Kolmogorov scale is a uniform straining rate of order  $(\varepsilon/\nu)^{1/2}$ , although then the constant remains undetermined. The corresponding dimensional argument applied to the scalar structure function  $\langle (\Delta_r \theta)^2 \rangle = \langle [\theta(\mathbf{x} + \mathbf{r}) - \theta(\mathbf{x})]^2 \rangle$  leads to the con-

<sup>a)</sup>Author to whom correspondence should be addressed. Electronic mail: brian.sawford@eng.monash.edu.au

clusion that  $\langle(\Delta_r\theta)^2\rangle$  is independent of the separation  $r$ .<sup>5,24</sup> However, the behavior of the structure function in the viscous-convective subrange is actually more complex and, as shown by Batchelor, has a logarithmic dependence on the separation

$$\langle(\Delta_r\theta)^2\rangle = 2\tilde{B}_\theta\chi(\nu/\varepsilon)^{1/2} \ln(r/\eta_B), \quad \eta_B \ll r \ll \eta. \quad (2)$$

Most studies of the viscous-convective subrange have focused on the spectral form Eq. (1) and have not addressed in detail the corresponding logarithmic form Eq. (2) for the structure function.

As a consequence of Eq. (1) Batchelor also noted that at sufficiently large Sc the scalar variance is dominated by the contribution from scales within the viscous-convective sub-range and is of order

$$\langle\theta^2\rangle = \frac{1}{2}\tilde{B}_\theta\chi(\nu/\varepsilon)^{1/2} \ln Sc, \quad (3)$$

and the time taken for a stationary state to develop with this variance is of order  $(\nu/\varepsilon)^{1/2} \ln Sc$ .

The work we present here is as follows. From an Eulerian view point, in Sec. II we emphasize the role of matching the scalar spectrum across the inertial-convective and viscous-convective subranges, thus relating the Obukhov-Corrsin constant in the inertial-convective subrange, the Batchelor constant in the viscous-convective subrange, and the wave number at which the two subranges match. We also discuss the more complex matching terms required for the structure function. Our exact Lagrangian analysis in terms of molecular trajectories for the case of a uniform mean scalar gradient in stationary isotropic turbulence is presented in Sec. III. It enables us to derive all of Batchelor's results directly in physical space and to provide a precise connection between the Batchelor constant and the Lyapunov exponent for pair separation in the dissipation subrange. In Sec. IV we reanalyze direct numerical simulation (DNS) results and present them in a form suitable for testing the predictions of the theory in physical space. Finally in Sec. V we discuss the significance of Batchelor's results, and of our analysis, in terms of both the explicit molecular corrections embodied in Eqs. (1)–(3), and perhaps more importantly, in terms of the so-called marked fluid particle limit, in which scalar statistics are related to the displacement statistics of fluid particles with no explicit consideration of molecular diffusion. Marked fluid particles are often used for descriptions of transport in turbulent flows on the basis that details of molecular properties can be ignored in the limit of extremely large Reynolds number. While widely accepted<sup>25–27</sup> the standard explanations for marked fluid particle representations of scalar mixing rely on heuristic arguments.<sup>28,29</sup> Here we have an explicit demonstration of the nature of the singular limit  $\kappa \rightarrow 0$ .

## II. EULERIAN ANALYSIS

### A. Preliminaries

Consider a stationary homogeneous scalar fluctuation field generated by turbulence acting on a uniform mean gradient of scalar,  $\langle\Theta(\mathbf{x},t)\rangle = mz$ . Note that we use both compo-

nent and Cartesian tensor notations  $(x,y,z)$  and  $(x_1,x_2,x_3)$ . There is now much evidence that such a scalar field is not isotropic, but for the second-order statistics that are of interest here the departure from isotropy is relatively small.<sup>30,31</sup> Here we assume isotropy and in order to minimize any effects of anisotropy in the data we present, we average over the three Cartesian components. The scalar fluctuation is  $\theta = \Theta - \langle\Theta\rangle$  and we can define the Eulerian scalar covariance as  $\langle\theta(\mathbf{x},t)\theta(\mathbf{x}+\mathbf{r},t)\rangle$ , which can be written in terms of the scalar spectrum as

$$\langle\theta(\mathbf{x},t)\theta(\mathbf{x}+\mathbf{r},t)\rangle = \int \phi_3(k)e^{ik\cdot r}d^3k = \int_0^\infty \phi(k)\frac{\sin kr}{kr}dk, \quad (4)$$

where  $\phi_3$  is the three-dimensional scalar spectrum,  $\phi(k) = 4\pi k^2\phi_3(k)$ , and the scalar variance is given by

$$\langle\theta^2\rangle = \int_0^\infty \phi(k)dk. \quad (5)$$

The scalar dissipation is

$$\chi = 2\kappa\left\langle\left(\frac{\partial\theta}{\partial x_i}\right)^2\right\rangle = 2\kappa\int_0^\infty \phi(k)k^2dk. \quad (6)$$

The transport equation for the scalar variance,

$$\frac{\partial\langle\theta^2\rangle}{\partial t} = P - \chi = -2m\langle\theta w\rangle - \chi, \quad (7)$$

allows the estimation of the stationary rate of dissipation of scalar fluctuations  $\chi$  at large times as a balance with the production of fluctuations  $P = -2m\langle\theta w\rangle$ ,

$$\chi = -2m\langle\theta w\rangle = 2m^2\kappa_t \quad (t \rightarrow \infty), \quad (8)$$

where  $\kappa_t$  is the turbulent diffusivity. We could regard the relation  $\langle\theta w\rangle = -\kappa_t m$  used in Eq. (8) as a definition of the turbulent diffusivity, but we will define it more precisely in Lagrangian terms in Sec. III.

We define a turbulence length scale by  $L = \sigma_w^3/\varepsilon$  where  $\sigma_w$  is the velocity component standard deviation. This turbulence length scale is related to the Kolmogorov and Batchelor length scales by

$$\eta = (\nu^3/\varepsilon)^{1/4} = L \text{Re}^{-3/4} \quad (9)$$

and

$$\eta_B = (\kappa^2\nu/\varepsilon)^{1/4} = L \text{Re}^{-3/4}\text{Sc}^{-1/2}, \quad (10)$$

where  $\text{Re} = \sigma_w L/\nu$  is the turbulence Reynolds number, which for isotropic turbulence is related to the commonly used Taylor scale Reynolds number  $\text{Re}_\lambda$  by  $\text{Re} = \text{Re}_\lambda^2/15$ . Corresponding to the turbulence length scale  $L$ , we can also define a time scale  $T_E = L/\sigma_w = \sigma_w^2/\varepsilon$ , which is related to the Kolmogorov time scale  $t_\eta = (\nu/\varepsilon)^{1/2}$  by

$$t_\eta = T_E \text{Re}^{-1/2}. \quad (11)$$

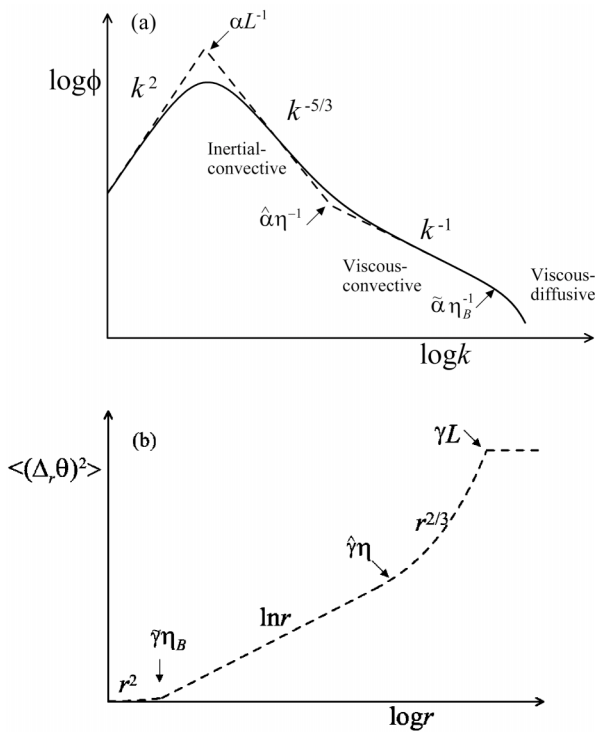


FIG. 1. Schematic piecewise continuous representations (dashed lines) of (a) the scalar variance spectrum and (b) the scalar second order structure function. In (a) the “actual” spectrum is shown schematically as the solid line.

**B. Piecewise continuous scalar spectrum**

The form of the scalar spectrum is well known in a number of wave number ranges. In the inertial-convective subrange  $L^{-1} \ll k \ll \eta^{-1}$ , we have the familiar result<sup>32–34</sup>  $\phi(k) = B_\theta \chi \varepsilon^{-1/3} k^{-5/3}$  where  $B_\theta$  is the Obukhov–Corrsin constant. In the viscous-convective subrange we have Batchelor’s result and in the viscous diffusive subrange where  $k \eta_B \gg 1$ , the spectrum falls off faster than algebraically. At large scales such that  $k \ll L^{-1}$  the form of the spectrum is less certain, but there is some basis for a power-law form  $\phi(k) \sim k^n$  with  $n = 2$  or  $4$ .<sup>35</sup> We will see that our results are not very sensitive to this uncertainty. Strictly these various subranges exist in statistical equilibrium only if (i) the Reynolds number and Schmidt number are large enough, (ii) there is a sufficiently large amount of variance in the large-scale subrange, and (iii) sufficient time is available to transfer scalar variance to the smallest scales. The latter two conditions are satisfied in the stationary state (when production equals dissipation) for scalar fluctuations in a uniform mean scalar gradient.

We can write down a simple piecewise continuous representation of the behavior [illustrated schematically in Fig. 1(a)] as

$$\phi(k) = \begin{cases} B_\theta \chi \varepsilon^{-1/3} \alpha^{-11/3} L^{11/3} k^2, & 0 \leq k \leq \alpha L^{-1} \\ B_\theta \chi \varepsilon^{-1/3} k^{-5/3}, & \alpha L^{-1} \leq k \leq \hat{\alpha} \eta^{-1} \\ \tilde{B}_\theta \chi (\nu/\varepsilon)^{1/2} k^{-1}, & \hat{\alpha} \eta^{-1} \leq k \leq \tilde{\alpha} \eta_B^{-1} \\ \leq C k^{-n} \forall n > 0 & \tilde{\alpha} \eta_B^{-1} \leq k, \end{cases} \quad (12)$$

where the numbers  $\alpha$ ,  $\hat{\alpha}$ , and  $\tilde{\alpha}$  are constants which reflect

the extent of the inertial-convective and viscous-convective subranges, and we have assumed a  $k^2$  behavior for the large scales. It follows from matching these two subranges at  $\tilde{\alpha} \eta^{-1}$  that  $\tilde{B}_\theta = B_\theta \hat{\alpha}^{-2/3}$ . Thus, not surprisingly the location of the crossover between the inertial-convective and viscous-convective subranges is determined by the ratio of the Batchelor constant and the Obukhov–Corrsin constant. We defer consideration of the numerical value of  $\hat{\alpha}$  to Sec. IV where we estimate the Batchelor constant from DNS results.

**C. The scalar variance**

The scalar variance in terms of the piecewise continuous spectrum is given by

$$\begin{aligned} \langle \theta^2 \rangle &= B_\theta \chi \varepsilon^{-1/3} \alpha^{-11/3} L^{11/3} \int_0^{\alpha L^{-1}} k^2 dk \\ &+ B_\theta \chi \varepsilon^{-1/3} \int_{\alpha L^{-1}}^{\hat{\alpha} \eta^{-1}} k^{-5/3} dk + \tilde{B}_\theta \chi (\nu/\varepsilon)^{1/2} \int_{\hat{\alpha} \eta^{-1}}^{\tilde{\alpha} \eta_B^{-1}} k^{-1} dk, \end{aligned} \quad (13)$$

where we have neglected the contribution from the tail beyond  $k = \tilde{\alpha} \eta_B^{-1}$ . Evaluating the integrals in Eq. (13) we have

$$\begin{aligned} \langle \theta^2 \rangle &= \frac{11}{6} B_\theta \chi \varepsilon^{-1/3} \alpha^{-2/3} L^{2/3} - \frac{3}{2} B_\theta \chi \varepsilon^{-1/3} \hat{\alpha}^{-2/3} \eta^{2/3} \\ &+ \tilde{B}_\theta \chi (\nu/\varepsilon)^{1/2} \ln(\tilde{\alpha}/\hat{\alpha}) + \frac{1}{2} \tilde{B}_\theta \chi (\nu/\varepsilon)^{1/2} \ln \text{Sc} \end{aligned} \quad (14)$$

which reduces to Batchelor’s result, Eq. (3), in the limit  $\text{Sc} \rightarrow \infty$  at finite  $\text{Re}$ . We can nondimensionalize the variance using the scalar dissipation and the turbulence time scale,

$$\begin{aligned} \frac{\langle \theta^2 \rangle}{\chi T_E} &= \frac{11}{6} B_\theta \chi \alpha^{-2/3} - \frac{3}{2} B_\theta \hat{\alpha}^{-2/3} \text{Re}^{-1/2} + \tilde{B}_\theta \text{Re}^{-1/2} \ln(\tilde{\alpha}/\hat{\alpha}) \\ &+ \frac{1}{2} \tilde{B}_\theta \text{Re}^{-1/2} \ln \text{Sc}, \end{aligned} \quad (15)$$

which shows that at large  $\text{Re}$  the  $\ln \text{Sc}$  term can only be significant for extreme values of the Schmidt number. However, if the Reynolds number is low and the Schmidt number is high, as can be the case in laboratory systems<sup>36</sup> there can be a significant practical effect on the variance due to the structure of the scalar field at very high wave numbers (due to the so-called filaments and sheets). We show in Sec. IV that significant perturbations may be observed if measuring instruments are able to resolve higher and higher wave numbers. However, in the limit of very large Reynolds number there is virtually no net effect on the estimate of scalar variance for practical diffusive substances and for finite  $\text{Sc}$  the variance asymptotes to a constant value given by the first term on the right,  $\langle \theta^2 \rangle_\infty / \chi T_E = \frac{11}{6} B_\theta \alpha^{-2/3}$ . This determines the number  $\alpha$ . Note that the integration of the inertial-convective subrange spectrum, i.e., the second term in Eq. (13), contributes 3/2 of the factor 11/6 (i.e., over 80%) of this asymptotic variance. Had we chosen a  $k^4$  behavior for the low wave number spectrum, the factor 11/6 would have been 17/10, which differs by less than 10% and would simply be reflected in a slightly different value for the constant  $\alpha$ .

The scalar dissipation rate can be calculated in spectral terms as  $2\kappa \int_0^\infty k^2 \phi(k) dk$  and in the case of large  $\text{Sc}$  and finite

Re can be estimated from the dominant contribution in the viscous-convective subrange, i.e., from the third line of Eq. (12), to give

$$\chi = 2\kappa\tilde{B}_\theta\chi t_\eta \int_0^{\tilde{\alpha}\tilde{\eta}_B^{-1}} kdk = \chi\tilde{B}_\theta\tilde{\alpha}^2, \quad (16)$$

which relates the cutoff to the viscous-convection subrange to the Batchelor constant through  $\tilde{B}_\theta\tilde{\alpha}^2=1$ . Thus we have estimates for all the numbers determining the extent of the inertial-convective and viscous-convection subranges in terms of the Obukhov–Corrsin and Batchelor constants and the large-Re limit of the scalar variance  $\langle\theta^2\rangle_\infty$ .

#### D. The spatial structure function

The two-point structure function in physical space is nontrivial in the viscous-convective subrange. We noted in the Introduction that a naïve dimensional argument implies that the structure function is constant there, but Batchelor showed that it has the logarithmic form Eq. (2). This can be derived from the Fourier transform of the  $k^{-1}$  spectrum suitably truncated at wave number  $\tilde{\alpha}\tilde{\eta}_B^{-1}$ . Details are given in the Appendix.

Adding the well-known behavior at very small scales,  $r \ll \eta_B$ , in the inertial-convective subrange,  $\eta \ll r \ll L$ , and at large scales  $r \gg L$ , we can construct a matched piecewise continuous approximation for the structure function [illustrated schematically in Fig. 1(b)] of the form

$$\langle(\Delta, \theta)^2\rangle = \begin{cases} \frac{1}{6}\chi t_\eta r^2 / \eta_B^2, & r \leq \tilde{\gamma}\eta_B \\ 2\tilde{B}_\theta\chi t_\eta \ln(r/\tilde{\gamma}\eta_B) + \frac{1}{6}\chi t_\eta \tilde{\gamma}^2, & \tilde{\gamma}\eta_B \leq r \leq \hat{\gamma}\eta \\ \sigma_\kappa^2 + C_\theta\chi\varepsilon^{-1/3}(r^{2/3} - \hat{\gamma}^{2/3}\eta^{2/3}), & \hat{\gamma}\eta \leq r \leq \gamma L \\ 2\sigma_L^2, & \gamma L \leq r, \end{cases} \quad (17)$$

where

$$\sigma_\kappa^2 = 2\tilde{B}_\theta\chi t_\eta \ln(\hat{\gamma}/\tilde{\gamma}) + \tilde{B}_\theta\chi t_\eta \ln \text{Sc} + \frac{1}{6}\chi t_\eta \tilde{\gamma}^2 \quad (18)$$

and

$$2\sigma_L^2 = 2\langle\theta^2\rangle = C_\theta\chi\varepsilon^{-1/3}(\gamma^{2/3}L^{2/3} - \hat{\gamma}^{2/3}\eta^{2/3}) + \sigma_\kappa^2. \quad (19)$$

The Obukhov–Corrsin constant in the structure function is related to the corresponding spectral constant<sup>34</sup> by  $C_\theta/B_\theta = 0.9\Gamma(1/3) \approx 2.41$ . As we foreshadowed in the Introduction, the matching corrections are more complex than for the spectrum.

Comparing Eqs. (19) and (14) for the scalar variance (based on the structure function and the spectrum, respectively) term by term, we can relate the numbers  $\alpha$ ,  $\hat{\alpha}$  and  $\tilde{\alpha}$  to  $\gamma$ ,  $\hat{\gamma}$  and  $\tilde{\gamma}$ , respectively, with the result

$$\begin{aligned} \alpha\gamma &= (5B_\theta/C_\theta)^{3/2} \approx 2.99, \\ \hat{\alpha}\hat{\gamma} &= \tilde{\alpha}\tilde{\gamma} = (3B_\theta/C_\theta)^{3/2} \approx 1.39. \end{aligned} \quad (20)$$

Note that the term  $\frac{1}{6}\chi t_\eta \tilde{\gamma}^2$  in Eq. (18) corresponds to the spectral integration over the tail beyond  $k = \tilde{\alpha}\tilde{\eta}_B^{-1}$  which we neglected in Eq. (14).

### III. SCALAR FLUCTUATIONS AS A LAGRANGIAN PROCESS

#### A. Overview

We now switch to a Lagrangian perspective of the scalar mixing process in which scalar concentration statistics are determined in terms of the displacement statistics of marked particles.<sup>37</sup> Since this approach will be unfamiliar to many readers, we first outline briefly the important concepts.

The theory is based on the displacement statistics of particles which move under the combined influence of the fluid motion and molecular diffusion according to the Ito stochastic differential equation<sup>38</sup>

$$dx_i = u_i(\mathbf{x}, \mathbf{u}, t)dt + \sqrt{2\kappa}dW_i, \quad (21)$$

where  $d\mathbf{W}$  is a vector incremental Wiener process.<sup>39</sup> Equation (21) describes the trajectory of a marked molecule, or alternatively the locus of the set of fluid elements which contain the marked molecule. Note that we do not use separate notations for Eulerian and Lagrangian quantities, relying on the context, and where necessary explicit use of the time argument, to identify Lagrangian quantities such as  $\mathbf{x}(t)$ . If we average over the molecular motions for a single realization  $\mathbf{u}^\omega$  of the flow field, then the displacement statistics satisfy the Fokker–Planck equation

$$\frac{\partial P^\omega}{\partial t} + u_i^\omega \frac{\partial P^\omega}{\partial x_i} = \kappa \frac{\partial^2 P^\omega}{\partial x_i^2}, \quad (22)$$

which is identical in form with the scalar conservation equation for incompressible flow. Thus for the initial condition  $P^\omega(\mathbf{x}, t'; \mathbf{x}', t') = \delta(\mathbf{x} - \mathbf{x}')$  on Eqs. (21) and (22) there is a precise correspondence between the displacement probability density function (PDF)  $P^\omega(\mathbf{x}, t; \mathbf{x}', t')$  and the instantaneous scalar concentration  $\Theta$  for an instantaneous point source of unit strength  $S(\mathbf{x}, t) = \delta(\mathbf{x} - \mathbf{x}')\delta(t - t')$ . Since Eq. (22) and the scalar conservation equation are linear, we can generalize this equivalence to an arbitrary source distribution  $S(\mathbf{x}, t)$  to give

$$\Theta(\mathbf{x}, t) = \int_V \int_{-\infty}^t P^\omega(\mathbf{x}, t; \mathbf{x}', t') S(\mathbf{x}', t') d\mathbf{x}' dt'. \quad (23)$$

We can then average over the flow field to calculate the moments of the scalar field in terms of the PDF  $P(\mathbf{x}, t; \mathbf{x}', t')$  for displacements due to the combined effects of the flow and molecular diffusion. Specifically we have

$$\overline{\Theta(\mathbf{x}, t)} = \int_V \int_{-\infty}^t P(\mathbf{x}, t; \mathbf{x}', t') S(\mathbf{x}', t') d\mathbf{x}' dt' \quad (24)$$

and

$$\begin{aligned} \overline{\Theta(\mathbf{x}_1, t_1)\Theta(\mathbf{x}_2, t_2)} &= \int_V \int_V \int_{-\infty}^{t_1} \int_{-\infty}^{t_2} P(\mathbf{x}_1, t_1, \mathbf{x}_2, t_2; \mathbf{x}'_1, t'_1, \mathbf{x}'_2, t'_2) \\ &\quad \times S(\mathbf{x}'_1, t'_1) S(\mathbf{x}'_2, t'_2) d\mathbf{x}'_1 d\mathbf{x}'_2 dt'_1 dt'_2. \end{aligned} \quad (25)$$

There are corresponding expressions for higher order moments but Eqs. (24) and (25) are sufficient for our present

purpose which is to calculate second order statistics of the scalar fluctuations. Equations (24) and (25) are cast in the so-called forward dispersion formulation (recognizing that  $t \geq t'$ ,  $t_1 \geq t'_1$ , and  $t_2 \geq t'_2$ ), but we will use the backwards formulation obtained from Eqs. (24) and (25) by substituting the relationships  $P(\mathbf{x}, t; \mathbf{x}', t') = P(\mathbf{x}', t'; \mathbf{x}, t)$  and  $P(\mathbf{x}_1, t_1, \mathbf{x}_2, t_2; \mathbf{x}'_1, t'_1, \mathbf{x}'_2, t'_2) = P(\mathbf{x}'_1, t'_1, \mathbf{x}'_2, t'_2; \mathbf{x}_1, t_1, \mathbf{x}_2, t_2)$  which are valid for incompressible flow.<sup>22,29</sup> The advantage in using the backwards formulation is that the concentration moments are then given as averages of products of the source distribution over the backwards displacement PDF.

The key to the exact results that we present below is the fact that the connection between marked particle displacements and the concentration variance (or covariance) is particularly simple for an instantaneous uniform gradient source in stationary homogeneous turbulence, since as we show in Sec. II B it involves only the difference between the dispersion of independent marked particles and half the relative dispersion of pairs of marked particles. At large times these two dispersion quantities are equal to the diffusion limit  $2\kappa_t t$ , where  $\kappa_t$  is the turbulent diffusivity, at leading order. Thus in order to calculate the stationary scalar variance and covariance at large times we need to consider the next order contribution to the pair dispersion.

Now we will show that for sufficiently large Schmidt number and sufficiently small initial separation the relative dispersion remains “trapped” within the dissipation subrange for a long time, thus essentially introducing a large lag time into the relative dispersion diffusion limit, so that the next order contribution can be determined in terms of this lag. In Sec. III C we calculate the relative dispersion exactly in this trapped phase and so are able to calculate the lag time explicitly, thus giving the leading estimates for the scalar variance and covariance in Sec. III D and III E. In so doing, we relate the Batchelor constant to the Lyapunov exponent<sup>27</sup> for the dispersion of pair trajectories in the dissipation subrange.

## B. Scalar variance and covariance in terms of marked particle statistics

To estimate the scalar variance at a point for a uniform gradient source switched on at time  $t=0$ ,  $S(\mathbf{x}, t) = m z \delta(t)$ , we have, using the backwards versions of Eqs. (24) and (25)<sup>28,37</sup>

$$\langle \theta^2 \rangle = m^2 \langle z^{(1)} z^{(2)} | \mathbf{r} = \mathbf{0} \rangle = m^2 \left( \langle z^2 \rangle - \frac{1}{2} \langle r_z^2 | \mathbf{r} = \mathbf{0} \rangle \right). \quad (26)$$

In this relation the Lagrangian  $z$  coordinates of the backwards displacements from the receptor (i.e., the positions at time  $t=0$  relative to the receptor at time  $t$ ) of a pair of particles are labeled  $z^{(1)}$  and  $z^{(2)}$ , respectively. The average  $\langle z^{(1)} z^{(2)} \rangle$  represents the covariance of the backwards  $z$  displacements of the two particles at time  $t=0$  given that both particles arrive at the receptor (which by homogeneity we can take to be  $\mathbf{x}=\mathbf{0}$ ) at time  $t$ . Similarly,  $\langle z^2 \rangle$  is the single particle dispersion for both particles (i.e.,  $\langle z^{(1)2} \rangle = \langle z^{(2)2} \rangle = \langle z^2 \rangle$  by homogeneity) and  $\langle r_z^2 | \mathbf{r} = \mathbf{0} \rangle = \langle (z^{(1)} - z^{(2)})^2 | \mathbf{r} = \mathbf{0} \rangle$  is the relative dispersion for the pair of particles. Our notation emphasizes that the relative dispersion depends on the separation at the receptor. In stationary homogeneous turbulence these dispersion quantities depend only on the magnitude of

the time difference and so are the same as the corresponding quantities at time  $t$  for particles which were at  $\mathbf{x}=\mathbf{0}$  at time  $t=0$ .

Similarly, we can estimate the scalar covariance by considering the backwards dispersion of pairs of particles which are at separate receptor points  $\mathbf{x}$  and  $\mathbf{x}+\mathbf{r}$  at time  $t$ ,

$$\begin{aligned} \langle \theta(\mathbf{x}) \theta(\mathbf{x} + \mathbf{r}) \rangle &= m^2 \langle z^{(1)} z^{(2)} | \mathbf{x}, \mathbf{x} + \mathbf{r} \rangle \\ &= m^2 \langle z^2 \rangle - \frac{1}{2} m^2 \langle r_z^2 | \mathbf{r} \rangle, \end{aligned} \quad (27)$$

where by homogeneity there is no dependence on  $\mathbf{x}$  and the single particle dispersion for each particle is identical.

The scalar production and dissipation can also be expressed in Lagrangian terms. Differentiating Eq. (26) with respect to time we have

$$\begin{aligned} \frac{d}{dt} \langle \theta^2 \rangle &= m^2 \frac{d}{dt} \langle z^2 \rangle - \frac{1}{2} m^2 \frac{d}{dt} \langle r_z^2 \rangle \\ &= 2m^2 (\kappa_t(t) + \kappa) - \frac{1}{2} m^2 \frac{d}{dt} \langle r_z^2 \rangle \\ &= -2m \langle w \theta \rangle + 2m^2 \kappa - \frac{1}{2} m^2 \frac{d}{dt} \langle r_z^2 \rangle, \end{aligned} \quad (28)$$

where by definition  $\kappa_t = \frac{1}{2} d \langle z^2 \rangle / dt - \kappa$  is the turbulent diffusivity. Comparing Eq. (28) with Eq. (7) for the scalar variance in homogeneous turbulence, we identify the first term of the third line on the right-hand side with the production term, so it follows that the scalar dissipation is given by

$$\chi = \frac{1}{2} m^2 \frac{d}{dt} \langle r_z^2 \rangle - 2m^2 \kappa. \quad (29)$$

## C. Molecular trajectories

The results given by Eqs. (26)–(29) are exact at all times for an instantaneous uniform gradient source in stationary homogeneous turbulence. We now turn to the calculation of these quantities using the exact equation (21) for molecular trajectories which can be solved formally in kinematic terms, and explicitly for relative motions within the dissipation subrange. We will focus on the large-time stationary state for the scalar statistics.

Equation (21) gives the displacement of a single particle along its trajectory. For the separation of a pair of particles  $\mathbf{r} = \mathbf{x}^{(1)}(t) - \mathbf{x}^{(2)}(t)$  we have

$$d\mathbf{r}_i = [u_i(\mathbf{x}^{(1)}, t) - u_i(\mathbf{x}^{(2)}, t)] dt + \sqrt{4\kappa} d\mathbf{W}_i^{(r)}, \quad (30)$$

where  $d\mathbf{W}^{(r)} = (d\mathbf{W}^{(1)} - d\mathbf{W}^{(2)}) / \sqrt{2}$  is also an incremental Wiener process (since the molecular motions of each particle are independent).

Now we can solve Eq. (21) to give the single particle dispersion<sup>40</sup>

$$\frac{1}{3} \langle x_i^2(t) \rangle = 2 \int_0^t \int_0^{t'} R_L^{(m)}(|t' - t''|) dt'' dt' + 2\kappa t, \quad (31)$$

where  $R_L^{(m)}(|t' - t''|) = \frac{1}{3} \langle u_j(t') u_j(t'') \rangle$  is the Lagrangian covariance of the fluid velocities at two times along the trajectory of a molecule. The superscript ( $m$ ) emphasizes that this is not

the same as the velocity covariance at different times along the trajectory of a fluid particle moving without the influence of molecular diffusion.

It follows from Eq. (31) that for large times the  $z$ -component dispersion is

$$\langle z^2 \rangle = 2\kappa_t t + 2\kappa t, \quad t \gg T_L^{(m)}, \quad (32)$$

where  $\kappa_t = \sigma_w^2 T_L^{(m)}$  is the turbulent diffusivity and  $T_L^{(m)}$  is the Lagrangian integral time scale for velocities along the molecular trajectory. Again, this is different from the Lagrangian integral time scale for fluid trajectories. We note as an aside that for arbitrary times  $t$  the turbulent diffusivity is obtained by differentiating (31) with respect to time to give  $\kappa_t = \frac{1}{2} d\langle z^2 \rangle / dt - \kappa = \int_0^t R_L^{(m)}(|t-t'|) dt'$ .

We cannot solve the separation equation exactly in general, but an exact solution is possible for separations which are much smaller than the Kolmogorov scale. Then the velocity field can be represented locally as a uniform gradient and Eq. (30) becomes<sup>27,41</sup>

$$dr_i = a_{ij}(\mathbf{x}^{(1)}, t) r_j dt + \sqrt{4\kappa d} W_i^{(r)}, \quad r \ll \eta, \quad (33)$$

where  $a_{ij}(\mathbf{x}, t) = \partial u_i / \partial x_j$  is the velocity gradient tensor and  $r^2 = r_i r_i$ . Using Ito's rule<sup>39</sup> we have

$$dr^2 = 2r^2 s dt + 12\kappa dt + 4r\sqrt{\kappa d} W^{(e)}, \quad r \ll \eta, \quad (34)$$

where  $s = e_i s_{ij} e_j$ ,  $dW^{(e)} = e_i dW_i^{(r)}$ , and  $\mathbf{e} = \mathbf{r}/r$  is the unit vector in the direction of the separation. For a fixed history  $S = \{s(t) | t \in [0, \infty)\}$  of  $s$ , i.e., for a given molecular trajectory  $\mathbf{x}^{(1)}(t)$ , we can average over the white noise  $dW^{(e)}$  to give

$$\frac{d}{dt} \langle r^2 | S \rangle = 2s \langle r^2 | S \rangle + 12\kappa, \quad r \ll \eta, \quad (35)$$

which after integration and then averaging over the trajectories  $\mathbf{x}^{(1)}(t)$  gives

$$\begin{aligned} \langle r^2 | r_0 \rangle &= r_0^2 \left\langle \exp\left(2 \int_0^t s(t') dt'\right) \right\rangle \\ &+ 12\kappa \int_0^t \left\langle \exp\left(2 \int_{t'}^t s(t'') dt''\right) \right\rangle dt', \end{aligned} \quad (36)$$

where  $r_0 \ll \eta$  is the initial separation of the pair of particles and our notation emphasizes the dependence on the initial separation.

Now, the velocity gradient is correlated over a time of order  $t_\eta$ , so for long times such that  $t \gg t_\eta$  the time integral  $\int_0^t s(t') dt'$  can be approximated as the sum of a large number  $N = t / (\beta t_\eta)$  of independent random variates, where  $\beta$  is a constant of order one. Thus as a result of the central-limit theorem,<sup>42</sup> the integral itself is a normally distributed random variable with mean  $\bar{s}t$  and variance  $\beta\sigma_s^2 t_\eta t$ , where  $\bar{s} = \lim_{t \rightarrow \infty} (1/t) \int_0^t s(t') dt'$  and  $\sigma_s$  is the standard deviation of  $s$ . Thus for any individual trajectory  $\mathbf{x}^{(1)}(t)$  the integral is given by

$$\int_0^t s(t') dt' = \bar{s}t + g\sqrt{t}, \quad (37)$$

where  $g$  is a Gaussian random variable with variance  $\beta\sigma_s^2 t_\eta$ . The different realizations of the trajectories  $\mathbf{x}^{(1)}(t)$  sample the Gaussian distribution of the variable  $g$ , so the average over trajectories corresponds to averaging over  $g$ , which leads to

$$\begin{aligned} &\left\langle \exp\left(2 \int_0^t s(t') dt'\right) \right\rangle \\ &= \frac{1}{\sqrt{2\pi\beta t_\eta \sigma_s}} \int_{-\infty}^{\infty} \exp[2(\bar{s}t + g\sqrt{t})] \exp\left(-\frac{g^2}{2\beta\sigma_s^2 t_\eta}\right) dg \\ &= \exp[2(\bar{s} + \beta\sigma_s^2 t_\eta)t], \end{aligned} \quad (38)$$

so finally we have

$$\begin{aligned} \langle r^2 | r_0 \rangle &= r_0^2 \exp(2\bar{s}t) + \frac{6\kappa}{\bar{s}} [\exp(2\bar{s}t) - 1] \\ &\approx \left(r_0^2 + \frac{6\kappa}{\bar{s}}\right) \exp(2\bar{s}t). \end{aligned} \quad (39)$$

The quantity  $\tilde{s} = 2\bar{s} + \beta\sigma_s^2 t_\eta$  is positive and in the limit of infinite Schmidt number is known as the Lyapunov exponent, an intrinsic Lagrangian property characterizing small-scale turbulence.<sup>27</sup> Note that both the Lagrangian mean  $\bar{s}$  and the fluctuations in  $s$  contribute to the growth in  $\langle r^2 \rangle$ .<sup>41</sup>

It is clear from Eq. (39) that we can keep  $\langle r^2 \rangle \ll \eta^2$  for an arbitrarily long time by making  $r_0$  and  $\kappa$  suitably small. Under these circumstances the assumptions underlying Eqs. (33) and (37) (i.e., that  $\langle r^2 \rangle \ll \eta^2$  and  $t \gg t_\eta$ ) are satisfied, so Eq. (39) is an exact result and we can use it to study the small-scale properties of the scalar concentration field at large Schmidt number through Eqs. (26) and (27). It is a simple explicit result which is a special case of the more formal and complex results described by Balkovsky and Fouxon<sup>43</sup> and Falkovich *et al.*<sup>27</sup>

### D. The concentration variance for large Schmidt number

Suppose now that the Schmidt number is very large and the separation of the receptor points vanishes,  $r_0 = 0$ . We see from Eq. (39) that the particle pair separation process is very slow to get going and it takes a time

$$t_\kappa = \frac{1}{2} \tilde{s}^{-1} \ln \frac{\eta^2}{6\kappa\tilde{s}} \approx \frac{1}{2} \tilde{s}^{-1} \ln \text{Sc} \quad (40)$$

for the separation to grow to a size of order  $\eta$ ; i.e., when  $\langle r^2(t_\kappa) | r_0 = 0 \rangle = \eta^2$ , where we have used  $\tilde{s} = \tilde{\beta}(\varepsilon/\nu)^{1/2}$  in the approximation on the right-hand side since as we have already noted the strain rate is of order  $\tilde{t}_\eta^{-1} = (\varepsilon/\nu)^{1/2}$ . Note the arbitrariness of the scale of order  $\eta$  does not affect this estimate for  $t_\kappa$ , since growth to a size  $C\eta$  merely adds a term  $\tilde{s}^{-1} \ln C$  which is negligible in the limit of large  $\text{Sc}$ , and we have ignored a term  $\frac{1}{2} \tilde{s}^{-1} \ln \tilde{\beta}/6$  for the same reason. During this long time for which  $\langle r^2 \rangle = \frac{1}{3} \langle r^2 \rangle$  remains small, the scalar dissipation Eq. (29) is negligible, but the production of scalar variance is unaffected and the fluctuations grow with the

one-particle displacement  $\langle z^2 \rangle$ , representing production with negligible dissipation. The time scale  $t_\kappa$  can also be interpreted as the time taken for the scalar variance to cross the spectrum from the production scales to the dissipative scales and can be estimated in a way analogous to Lumley's<sup>44</sup> calculation for the turbulence spectrum.

In the long-time limit,  $t \approx t_\kappa \gg T_L^{(m)}$  the single particle dispersion is given by the simple diffusion result Eq. (32) at leading order and the scalar variance thus grows like

$$\langle \theta^2 \rangle = 2m^2 \kappa t \quad (41)$$

indicating that the fluctuations will grow without bound if the relative dispersion is always negligible. But this can only be true for a finite time and the estimate of the time scale for the equilibration of the variance is the critical aspect of this problem.

For times larger than  $t_\kappa$  relative dispersion proceeds under the influence of inertial-convective subrange eddies and ultimately the energy-containing eddies, so that eventually the pair separation is a diffusion process too, with  $\langle r_z^2 \rangle \sim 4\kappa_t(t - t_\kappa)$ , where the lag  $t_\kappa$  reflects the fact that negligible separation occurs over this time. This represents a model for separation behavior that has effectively negligibly small separations within the dissipation subrange for all times less than the critical time scale  $t_\kappa$ , but with linear turbulent diffusion for rapid pair separation after the critical time. Note that the pair separation cannot be more rapid than the independent one-particle turbulent dispersion. The transition regime between these two distinct behaviors occurs on the relatively small time scale measured by  $T_L^{(m)}$  with details that do not affect the leading order scaling results.

A piecewise continuous match to Eq. (39) gives the useful result

$$\langle r_z^2 | r_0 = 0 \rangle = \begin{cases} \frac{1}{3} \eta^2 \exp[2\tilde{s}(t - t_\kappa)], & t_\eta \ll t \leq t_\kappa, \\ 4\kappa_t(t - t_\kappa) + \frac{1}{3} \eta^2, & t \geq t_\kappa. \end{cases} \quad (42)$$

We obtain an accurate leading order estimate for the stationary scalar variance for  $t \gg t_\kappa$  by substituting Eq. (32) (neglecting the molecular diffusion term) and the second line of Eq. (42) in Eq. (26) to give

$$\langle \theta^2 \rangle \approx 2m^2 \kappa_t t_\kappa \approx \kappa_t m^2 \tilde{s}^{-1} \ln \text{Sc} \\ = \frac{1}{2} \chi \tilde{\beta}^{-1} t_\eta \ln \text{Sc} \quad (\text{Sc} \rightarrow \infty), \quad (43)$$

where we have used (8) for the scalar dissipation rate in the stationary state. Comparing Eq. (43) with Eq. (14) we see that

$$\tilde{B}_\theta = \tilde{\beta}^{-1}, \quad (44)$$

thus relating the Batchelor constant, a parameter of the Eulerian scalar variance spectrum, to the Lyapunov exponent.

### E. The concentration structure function for large Schmidt number

For nonzero initial separations much smaller than the microscale  $\eta$ , there is also a long-time dispersion regime for which the pair separation is small and we find from Eq. (39) that the separation is of order  $\eta$  after a time

$$t_{r_0} = \frac{1}{2} \tilde{s}^{-1} \ln \frac{\eta^2}{r_0^2 + 6\kappa/\tilde{s}}, \quad (45)$$

which is smaller than  $t_\kappa$  in Eq. (40) because of the nonzero initial separation  $r_0$ . As in the preceding section we then have the relative dispersion piecewise continuous approximation

$$\langle r_z^2 | r_0 \rangle = \begin{cases} \frac{1}{3} \eta^2 \exp[2\tilde{s}(t - t_{r_0})], & t_\eta \ll t \leq t_{r_0}, \\ 4\kappa_t(t - t_{r_0}) + \frac{1}{3} \eta^2, & t \geq t_{r_0}. \end{cases} \quad (46)$$

Now, from the second lines of both Eqs. (26) and (27) we have for the structure function

$$\langle (\Delta_{r_0} \theta)^2 \rangle = 2\langle \theta^2 \rangle - 2\langle \theta(\mathbf{x}) \theta(\mathbf{x} + \mathbf{r}_0) \rangle \\ = \langle r_z^2 | r_0 \rangle - \langle r_z^2 | r_0 = 0 \rangle. \quad (47)$$

Substituting Eqs. (42) and (46) gives the steady-state structure function in the long-time limit ( $t \gg t_\kappa > t_{r_0}$ )

$$\langle (\Delta_{r_0} \theta)^2 \rangle = 4m^2 \kappa_t t_\kappa - 4m^2 \kappa_t t_{r_0} \\ = \chi \tilde{s}^{-1} \ln \frac{\eta^2}{6\kappa/\tilde{s}} - \chi \tilde{s}^{-1} \ln \frac{\eta^2}{r_0^2 + 6\kappa/\tilde{s}}, \quad (48)$$

where again we have used Eq. (8) for the scalar dissipation in the stationary state. In the limit  $r_0 \ll \eta_B \propto \sqrt{\kappa/\tilde{s}}$  we have

$$\langle (\Delta_{r_0} \theta)^2 \rangle = \frac{\chi}{6\kappa} r_0^2, \quad r_0 \ll \eta_B \quad (49)$$

which is exact and is equivalent to the first regime of the result Eq. (17) derived from the Eulerian spectrum.

For  $\eta_B \ll r_0 \ll \eta$  Eq. (48) reduces at leading order to

$$\langle (\Delta_{r_0} \theta)^2 \rangle = 2\chi \tilde{B}_\theta t_\eta \ln(r_0/\eta_B), \quad \eta_B \ll r_0 \ll \eta \quad (50)$$

which is equivalent to the second regime of Eq. (17).

## IV. DNS RESULTS

Scalar concentration statistics for a uniform gradient source in forced isotropic turbulence have been reported recently.<sup>3,4,9,45</sup> Other works deal with an isotropically forced scalar field<sup>1</sup> or with a decaying scalar field in decaying turbulence.<sup>5,7</sup> Here we use results reported by Overholt and Pope,<sup>45</sup> and a reanalysis of data reported by Yeung *et al.*<sup>3,4</sup> in an attempt to test the theoretical estimates presented in Secs. II and III. We focus on the nature of the structure function in the viscous-convective subrange and on the dependence of the scalar variance on both Re and Sc.

Figure 2 shows a reanalysis of the normalized second order scalar structure function from the results of Yeung *et al.*<sup>3</sup> at  $\text{Re}_\lambda = 38$  and of Yeung *et al.*<sup>4</sup> at  $\text{Re}_\lambda = 8$ . In both panels of the figure the data collapse to the exact quadratic results Eq. (49) for  $r/\eta_B < 3$ . The log-linear plot shows the viscous-convective subrange as a linear region that extends to larger scales with increasing Sc. In Fig. 2(a) for  $\text{Re}_\lambda = 8$  the lines extend up to  $\text{Sc} = 1024$  at grid resolutions from  $128^3$  to  $512^3$  and show an increasing tendency to collapse onto a common line with increasing Sc. For  $\text{Sc} = 64$  the curves at  $128^3$  and  $256^3$  resolution agree fairly well, but there is an offset for the curves at  $256^3$  and  $512^3$  resolution for  $\text{Sc} = 256$ , probably

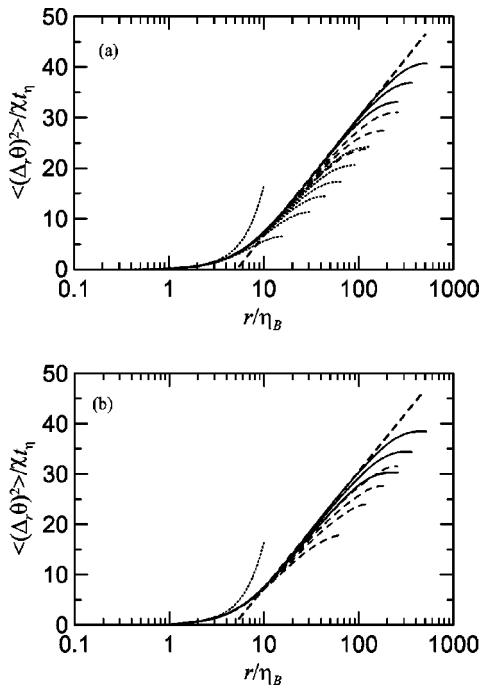


FIG. 2. Scalar structure function  $\langle (\Delta_r \theta)^2 \rangle / \chi t_\eta$  as a function of  $r/\eta_B$  for (a)  $Re_\lambda=8$  and (from the bottom)  $Sc=1, 4, 8, 16, 32, 64$  on a  $128^3$  grid (.....),  $Sc=64, 128,$  and  $256$  on a  $256^3$  grid (- - -), and  $Sc=256, 512,$  and  $1024$  on a  $512^3$  grid (—) and (b)  $Re_\lambda=38$  and (from the bottom)  $Sc=1, 4, 8,$  and  $16$  on a  $256^3$  grid (- - -) and  $Sc=16, 32,$  and  $64$  on a  $512^3$  grid (—). In both panels, the straight dashed line is the function  $a \ln(r/\eta_B) + b$  fitted to the highest  $Sc$  curve over the near-linear range in the plot and the concave-up dotted curve is the function  $\frac{1}{6}(r/\eta_B)^2$ .

because the large scales are less well sampled in the higher resolution run where computational expense limits the period of the integration (see also the discussion of Fig. 3 below). The straight dashed line is the function  $10.2 \ln(r/\eta_B) - 16.7$  with coefficients determined by a fit to the  $Sc=1024$  data for  $10 \leq r/\eta_B \leq 100$ . The same behavior is observed at  $Re_\lambda=38$  in Fig. 2(b), but these results are available only for  $1 \leq Sc \leq 64$ . In this case the fitted line is  $10.1 \ln(r/\eta_B) - 15.9$ . The manifestation of the viscous-convective regime in these plots seems to be much clearer than occurs on the corresponding spectral plots seeking to display the  $k^{-1}$  behavior.<sup>3,4,6</sup> The

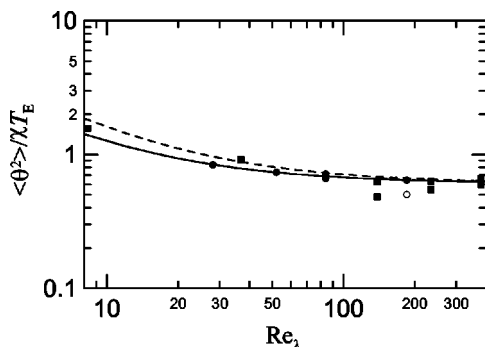


FIG. 3. Nondimensional scalar variance as a function of Reynolds number. Symbols are for DNS data of Overholt and Pope (Ref. 45) (●, ○) and Yeung *et al.* (Refs. 3 and 4) (■). The solid line and dashed lines are the functions  $0.61 + 6.5 Re_\lambda^{-1}$  and  $0.61 + 10 Re_\lambda^{-1}$ , respectively.

TABLE I. Transition numbers quantifying the extent of the inertial-convective and viscous-convective subranges.

$\hat{\alpha}$ $= (B_\theta / \tilde{B}_\theta)^{3/2}$	$\tilde{\alpha}$ $= \tilde{B}_\theta^{-1/2}$	$\hat{\gamma}$ $= (3B_\theta / C_\theta)^{3/2} / \hat{\alpha}$	$\tilde{\gamma}$ $= (3B_\theta / C_\theta)^{3/2} / \tilde{\alpha}$	$\alpha = (\frac{11}{6} B_\theta \chi T_E / \langle \theta^2 \rangle_\infty)^{3/2}$
0.049	0.45	28	3.1	2.9

inertial-convective region is completely absent at the Reynolds numbers of Fig. 2 [cf. the schematic in Fig. 1(b)].

Both the fits in Fig. 2 have high precision, but it is likely that the coefficients, particularly at  $Re_\lambda=8$ , are subject to some uncertainty associated with the limited sampling available in the relatively short runs at the highest resolution. According to Eqs. (17) or (50) the slope of the viscous-convective region in these log-linear plots is equal to  $2\tilde{B}_\theta$ , so from the fits in Fig. 2 we estimate  $\tilde{B}_\theta \approx 5$ . Also from Eq. (17) we have the theoretical estimate  $-2\tilde{B}_\theta \chi t_\eta \ln(\tilde{\gamma}) + \frac{1}{6} \chi t_\eta \tilde{\gamma}^2$  for the constant offset in the fits in Fig. 2, which we can calculate once we have determined a value for the matching constant  $\tilde{\gamma}$ .

From estimates for the Batchelor constant and the Obukhov–Corrsin constant  $B_\theta$  we can evaluate the numbers  $\hat{\alpha}$ ,  $\tilde{\alpha}$ ,  $\hat{\gamma}$ , and  $\tilde{\gamma}$  which determine the limits of the viscous-convective subrange in spectral and physical space in Eqs. (12) and (17), respectively. Table I summarizes the values of these numbers corresponding to  $\tilde{B}_\theta=5$  with  $B_\theta=0.67$  (Ref. 46) and  $C_\theta=1.61$ . Using the value  $\tilde{\gamma}=3.1$  we find that according to Eq. (17) the constant offset in the viscous-convective subrange is  $-9.7$ , about 40% lower than the fitted values from Fig. 2. This discrepancy is probably due to the lack of a well-resolved inertial-convective subrange at these low Reynolds numbers (see below).

From Table I, we expect the transition from the quadratic result Eq. (49) to the viscous-convective subrange to occur near  $r/\eta_B=3.1$  and if the Reynolds number were high enough the transition to the inertial-convective subrange would occur near  $r/\eta=28$  or equivalently  $r/\eta_B=28 Sc^{1/2}$ . Although the Reynolds number is not high enough to display an inertial-convective subrange in Fig. 2, and therefore the large-scale end of the viscous-convective subrange is truncated by the energy-containing scales, the large value of the ratio  $\hat{\gamma}/\tilde{\gamma}$  means that the extent of the viscous-convective subrange tends to be an order of magnitude larger than the simple estimate  $\eta/\eta_B=Sc^{1/2}$ . Furthermore, although the results for  $Sc=1$  do not collapse onto the limiting line, the increased separation of scales implied by the  $\gamma$  ratio means that there is still a tendency to show an incipient linear viscous-convective region in these plots, more so for the higher  $Re$  case in Fig. 2(b). This increased separation of scales, represented in spectral terms by the ratio  $\tilde{\alpha}/\hat{\alpha}$ , also explains the “spectral bump” observed in compensated spectral plots at  $Sc=1$  (see, e.g., Fig. 1 of Yeung *et al.*<sup>3</sup>) as the onset of a viscous-convective region.

We now turn to the concentration variance as a function of Schmidt number and Reynolds number. In particular, since we now have estimates for the Batchelor constant, the Obukhov–Corrsin constant and the transition numbers, we

TABLE II. Turbulence and scalar variables calculated from the DNS runs of Yeung *et al.* (Refs. 3 and 4).

$Re_\lambda$	Sc	Grid	$\chi$	$t_\eta$	$K$	$\varepsilon$	$\langle \theta^2 \rangle$
8	1	128	2.08	0.240	2.13	2.76	1.68
8	4	128	2.33	0.240	2.13	2.76	3.21
8	8	128	2.36	0.240	2.13	2.76	4.11
8	16	128	2.40	0.240	2.13	2.76	5.01
8	32	128	2.41	0.240	2.13	2.76	5.96
8	64	128	2.39	0.240	2.13	2.76	6.93
8	64	256	2.25	0.243	2.07	2.73	6.50
8	128	256	2.24	0.243	2.07	2.73	7.45
8	256	256	2.23	0.243	2.07	2.73	8.40
8	256	512	2.47	0.24	2.12	2.80	9.88
8	512	512	2.45	0.24	2.12	2.80	10.91
8	1024	512	2.43	0.24	2.12	2.80	11.94
38	1	256	2.50	0.094	3.78	2.80	2.05
38	4	256	2.72	0.097	3.76	2.68	3.09
38	8	256	2.73	0.097	3.76	2.68	3.58
38	16	256	2.73	0.097	3.76	2.68	4.09
38	16	512	2.74	0.096	3.96	2.75	4.06
38	32	512	2.73	0.096	3.96	2.75	4.58
38	64	512	2.73	0.096	3.96	2.75	5.12
140	0.125	256	1.95	0.049	3.09	1.18	1.64
140	1	256	2.00	0.049	3.09	1.18	2.19
240	0.125	512	3.27	0.03	3.35	1.24	3.22
240	1	512	3.30	0.03	3.35	1.24	3.73
390	0.125	512	2.46	0.0185	3.58	1.29	2.66
390	1	512	2.41	0.0185	3.58	1.29	2.89

can explicitly test the piecewise integrated estimate (15) for the scalar variance.

For the values of  $\hat{\alpha}$  and  $\tilde{\alpha}$  given in Table I Eq. (15) becomes

$$\frac{\langle \theta^2 \rangle}{\chi T_E} = \frac{11}{6} B_\theta \alpha^{-2/3} + 0.71 \sqrt{15 \tilde{B}_\theta} Re_\lambda^{-1} + \frac{1}{2} \sqrt{15 \tilde{B}_\theta} Re_\lambda^{-1} \ln Sc. \quad (51)$$

With  $\tilde{B}_\theta=5$  the coefficient of the combined  $Re_\lambda^{-1}$  terms in Eq. (51) is 10 for  $Sc=0.7$  and 14 for  $Sc=1$ .

Figure 3 shows a plot of the scalar variance, nondimensionalized as in Eq. (15), as a function of  $Re_\lambda$  for the data of Overholt and Pope<sup>45</sup> at  $Sc=0.7$  and for the data from the DNS runs of Yeung *et al.*<sup>3</sup> at  $Sc=1$ , summarized in Table II. Note that for the Overholt and Pope data we have doubled their quoted values for  $\chi$  to bring them into line with the definition Eq. (6) used here. We also estimated  $\chi$  separately using their data for the scalar flux and the relation Eq. (8), anticipating that the flux is more reliably sampled than the dissipation itself. There are thus two points plotted in Fig. 3 for each run reported for their data, although the differences are only significant at the largest Reynolds number which is for a single realization and where the point calculated using the direct estimate for  $\chi$  lies below the trend line. The solid line in Fig. 3 is the function  $0.61 + 6.5 Re_\lambda^{-1}$ , which is a good fit to the Overholt and Pope data, but the coefficient of the  $Re_\lambda^{-1}$  term is about 60% smaller than our estimate from Eq.

(51). Again this discrepancy is probably due to the lack of a well-resolved inertial-convective subrange at these low Reynolds numbers. There is consistency between the data of Overholt and Pope and Yeung *et al.*, with the latter lying a little higher on the plot at low Reynolds number, due to the effect of the term involving the Schmidt number in Eq. (51). Thus, the dashed line in Fig. 3 is derived from the solid line simply by subtracting the term involving the Schmidt number  $\frac{1}{2} \sqrt{15 \tilde{B}_\theta} Re_\lambda^{-1} \ln 0.7 = -3.5 Re_\lambda^{-1}$ .

The fitted value  $\langle \theta^2 \rangle_\infty / \chi T_E \approx 0.61$  for the large Reynolds number limit of the nondimensional scalar variance gives a value  $\alpha=2.9$  for the number defining the large scale limit of the inertial-convective subrange. Thus we can estimate the extent of the spectral inertial-convective subrange as  $\hat{\alpha} \eta^{-1} / \alpha L^{-1} = 1.7 \times 10^{-2} Re_\lambda^{3/4}$ , so that the inertial-convective subrange disappears completely for  $Re_\lambda \leq 60$ . This is consistent with DNS results shown as a compensated spectrum plot in Fig. 1 of Yeung *et al.*<sup>3</sup> About half of our Fig. 3 is for  $Re_\lambda \leq 60$ , so the discrepancy with Eq. (51) is not surprising. It is perhaps encouraging that a simple parameterization describes the data so well.

In Fig. 4 we show the nondimensional scalar variance as a function of Schmidt number for the data of Yeung *et al.*<sup>4</sup> at  $Re_\lambda=8$ , Yeung *et al.*<sup>3</sup> at  $Re_\lambda=38, 140, 240$  (summarized in Table II) and Overholt and Pope<sup>45</sup> for various values of Reynolds number at  $Sc=0.7$ . The solid lines have been plotted using the function

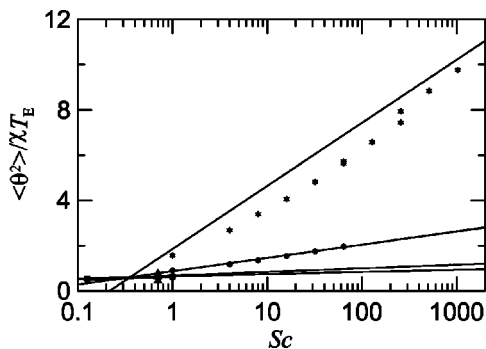


FIG. 4. Nondimensional scalar variance as a function of Schmidt number. The symbols are for DNS data of Yeung *et al.* (Ref. 4) at  $Re_\lambda=8$  (★), Yeung *et al.* (Ref. 3) at  $Re_\lambda=38$  (●), 140 (■) and 240 (◆) and Overholt and Pope (Ref. 45) (▲) for various Reynolds numbers and  $Sc=0.7$ . The solid lines are evaluated from (52).

$$\frac{\langle \theta^2 \rangle}{\chi T_E} = 0.61 + 10Re_\lambda^{-1} + \frac{1}{2} \tilde{B}_\theta \sqrt{15} Re_\lambda^{-1} \ln Sc \quad (52)$$

with  $\tilde{B}_\theta=5$ . These lines are thus constrained to pass through the corresponding data for  $Sc=1$ , consistent with the fit in Fig. 3. For moderate values of the Schmidt number the lines defined by Eq. (52) lie above the data, more conspicuously so at  $Re_\lambda=8$  but the data and the lines appear to be converging in the limit of large Schmidt number. Notice also the small offset in the  $Sc=256$  results at the two different resolutions for  $Re_\lambda=8$ , corresponding to the offset at large scales in the structure function results discussed above for Fig. 2. The consistency between Figs. 2 and 4, both in confirming the presence of the Batchelor subrange and in the value implied for the Batchelor constant, is encouraging.

Figure 4 and Eq. (52) quantify the effect of Schmidt number on the scalar variance, showing clearly that at low Reynolds numbers the variance is strongly influenced by Schmidt number. The effect is dramatic at very low Reynolds number, but for  $Sc=770$  (salt in water) even at  $Re_\lambda=400$  (i.e.,  $Re > 10^4$ ), which is typical of laboratory systems,<sup>36</sup> the Schmidt number term adds 25% to the variance.

### V. CONCLUSIONS

We have demonstrated the existence of Batchelor’s viscous-convective subrange using DNS results to confirm the logarithmic dependence of the scalar structure function on the separation  $r$  for the scalar field generated by stationary isotropic turbulence acting on a uniform mean scalar gradient. From these data we estimate the Batchelor constant to take a value of  $\approx 5$  at large Schmidt numbers. By integrating a piecewise continuous representation of the scalar variance spectrum we calculated the steady-state scalar variance through Eq. (15) as a function of Reynolds number and Schmidt number. Comparison with the DNS results of Overholt and Pope<sup>45</sup> and Yeung *et al.*<sup>3,4</sup> confirms the  $Re_\lambda^{-1}$  behavior predicted from the spectral integration, but with a coefficient about 60% too small. This may be due to the lack of an inertial-convective subrange at Reynolds numbers low enough for the  $Re_\lambda^{-1}$  correction term to be significant. In the large Reynolds number limit the data give a value

$\langle \theta^2 \rangle_\infty / \chi T_E \approx 0.61$  for the variance. This is equivalent to the value  $K\chi/\varepsilon \langle \theta^2 \rangle_\infty \approx 2.5$  for the commonly used mechanical-to-scalar time scale ratio, where  $K$  is the turbulence kinetic energy, and is thus consistent with an earlier analysis<sup>47</sup> of some of these data. The dependence of the data for the variance on Schmidt number on the other hand agrees very well with the spectral integration using the values of the Batchelor constant estimated from the structure function. We have thus demonstrated a consistent picture for these related, but different, scalar statistics.

The piecewise continuous representation of the scalar spectrum also enabled us to quantify the extent of the inertial-convective and viscous-convective subranges, in both spectral and physical space, in terms of the values taken for the Obukhov–Corrsin constant, the Batchelor constant and the asymptotic scalar variance  $\langle \theta^2 \rangle_\infty$ . We found that the viscous-convective subrange is an order of magnitude wider than the simple estimate  $\eta/\eta_B=Sc^{1/2}$ , and that the inertial-convective subrange (in spectral terms) is two orders of magnitude narrower than the simple estimate  $L/\eta=Re^{3/4}$  and is completely nonexistent for  $Re_\lambda \leq 60$ .

We also carried out an exact Lagrangian analysis of the scalar variance and structure function, explicitly relating the Batchelor constant to the Lyapunov exponent for the separation of pairs of fluid particles within the turbulence dissipation subrange.

Our results, particularly Eq. (52) for the scalar variance, illustrate explicitly the singular nature of the limit  $\kappa \rightarrow 0$ . For  $Sc \rightarrow \infty$  at finite  $Re$  the stationary scalar variance is infinite, but is not reached in a finite time. In this case particle pairs with vanishing initial separation remain together forever and there is no dissipation of scalar variance (in the limit) which grows indefinitely as in Eq. (41), i.e.,  $\langle \theta^2 \rangle = 2m^2 \kappa t$  for large times. This corresponds to the continual sharpening of scalar gradients by the stretching and folding action of the turbulence.

On the other hand, for  $Re \rightarrow \infty$  at finite  $Sc$  the scalar variance is given by the asymptotic value  $\langle \theta^2 \rangle_\infty$  which is independent of molecular diffusion and corresponds to an inertial-convective subrange extending to arbitrarily small scales. This is the limit obtained in a Lagrangian sense by the backwards relative dispersion of pairs of fluid particles whose separation at the measurement time vanishes on inertial range scales while remaining much larger than the Kolmogorov scale. Through the second term on the right-hand side of Eq. (13) the inertial-convective subrange of the scalar spectrum contributes more than 80% of the variance  $\langle \theta^2 \rangle_\infty$  which thus depends explicitly on the inertial subrange relative dispersion process.

For finite values of  $Sc$  and  $Re$ , the viscous-convective subrange contribution to the variance can be significant even at moderate values of the Reynolds number.

In future work we hope to improve our estimates for the Batchelor constant by (i) improved sampling of the existing high resolution runs, (ii) the use of Lagrangian methods to calculate the scalar variance and covariance, possibly at higher Reynolds and Schmidt numbers than achieved here,

and (iii) direct Lagrangian calculation of the Lyapunov coefficient.

## ACKNOWLEDGMENTS

This work was supported in part by the U.S. National Science Foundation, Grant No. CTS-0121030 (awarded to P.K.Y.), as well as via NSF cooperative agreement ACI-9619020 through computing resources provided by the National Partnership for Advanced Computational Infrastructure at the San Diego Supercomputer Center. Much of the work was carried out while B.L.S. was employed by CSIRO.

## APPENDIX: FOURIER TRANSFORM OF VISCOUS-CONVECTIVE SPECTRUM

From (4) and (12), the structure function in the viscous-convective range is given by

$$\langle(\Delta_r\theta)^2\rangle = 2\tilde{B}_\theta\chi\left(\frac{\nu}{\varepsilon}\right)^{1/2} \int_0^\infty k^{-1}f(k)\left(1 - \frac{\sin kr}{kr}\right)dk, \quad (\text{A1})$$

where  $f(k)$  is a faster than algebraic cut off “located” at  $k = \tilde{\alpha}\eta_B^{-1}$  such that  $f(0)=1$  and  $f(\infty)=0$ . Differentiating with respect to  $r$ , Eq. (A1) can be written as

$$\frac{d}{dr}\langle(\Delta_r\theta)^2\rangle = -2r^{-1}\tilde{B}_\theta\chi\left(\frac{\nu}{\varepsilon}\right)^{1/2} \int_0^\infty f(k)\frac{d}{dk}\left(\frac{\sin kr}{kr}\right)dk. \quad (\text{A2})$$

Integrating by parts we have

$$\frac{d}{dr}\langle(\Delta_r\theta)^2\rangle = 2r^{-1}\tilde{B}_\theta\chi\left(\frac{\nu}{\varepsilon}\right)^{1/2} \left(1 + \int_0^\infty f'(k)\frac{\sin kr}{kr}dk\right). \quad (\text{A3})$$

For a suitably sharp cutoff function, its derivative  $f'$  will be sharply peaked about  $r = \tilde{\alpha}^{-1}\eta_B$  (for example, it would be a  $\delta$  function for a step function cutoff) so the remaining integral can be approximated as  $\sin r\tilde{\alpha}\eta_B^{-1}/r\tilde{\alpha}\eta_B^{-1}$  and is negligible in the viscous-convection range where  $r \gg \eta_B$ . Thus we have finally

$$\langle(\Delta_r\theta)^2\rangle = 2\tilde{B}_\theta\chi\left(\frac{\nu}{\varepsilon}\right)^{1/2} \ln\frac{r}{\eta_B}. \quad (\text{A4})$$

<sup>1</sup>D. Bogucki, J. A. Domaradzki, and P. K. Yeung, “Direct numerical simulations of passive scalars with  $Pr > 1$  advected by turbulent flow,” *J. Fluid Mech.* **343**, 111 (1997).

<sup>2</sup>W. D. Smyth, “Dissipation-range geometry and scalar spectra in sheared stratified turbulence,” *J. Fluid Mech.* **401**, 209 (1999).

<sup>3</sup>P. K. Yeung, S. Xu, and K. R. Sreenivasan, “Schmidt number effects on turbulent transport with uniform mean scalar gradient,” *Phys. Fluids* **14**, 4178 (2002).

<sup>4</sup>P. K. Yeung, S. Xu, D. A. Donzis, and K. R. Sreenivasan, “Simulations of three-dimensional turbulent mixing of Schmidt numbers of the order 1000,” *Flow, Turbul. Combust.* **72**, 333 (2004).

<sup>5</sup>R. A. Antonia and P. Orlandi, “Dependence of the second-order scalar structure function on the Schmidt number,” *Phys. Fluids* **14**, 1552 (2002).

<sup>6</sup>R. A. Antonia and P. Orlandi, “On the Batchelor constant in decaying isotropic turbulence,” *Phys. Fluids* **15**, 2084 (2003).

<sup>7</sup>P. Orlandi and R. A. Antonia, “Dependence of the non-stationary form of Yaglom’s equation on Schmidt number,” *J. Fluid Mech.* **451**, 99 (2003).

<sup>8</sup>G. Brethouwer, “Mixing of passive and reactive scalars in turbulent flows: A numerical study,” Ph.D. thesis, Delft University of Technology, 2000.

<sup>9</sup>G. Brethouwer, J. C. R. Hunt, and F. T. M. Nieuwstadt, “Micro-structure and Lagrangian statistics of the scalar field with a mean gradient in isotropic turbulence,” *J. Fluid Mech.* **474**, 193 (2003).

<sup>10</sup>K. A. Buch and W. J. A. Dahm, “Experimental study of the fine-scale structure of conserved scalar mixing in turbulent shear flows. Part 1,  $Sc \gg 1$ ,” *J. Fluid Mech.* **317**, 21 (1996).

<sup>11</sup>P. S. Karasso and M. G. Mungal, “Scalar mixing and reaction in plane liquid shear layers,” *J. Fluid Mech.* **323**, 23 (1996).

<sup>12</sup>H. J. Catrakis and P. E. Dimotakis, “Mixing in turbulent jets: scalar measures and isosurface geometry,” *J. Fluid Mech.* **317**, 369 (1996).

<sup>13</sup>G. K. Batchelor, “Small-scale variation of convected quantities like temperature in a turbulent fluid,” *J. Fluid Mech.* **5**, 113 (1959).

<sup>14</sup>C. H. Gibson and W. H. Schwarz, “The universal equilibrium spectra of turbulent velocity and scalar fields,” *J. Fluid Mech.* **16**, 365 (1963).

<sup>15</sup>R. R. Prasad and K. R. Sreenivasan, “Quantitative three-dimensional imaging and the structure of passive scalar fields in fully turbulent flows,” *J. Fluid Mech.* **216**, 1 (1990).

<sup>16</sup>P. M. Miller and P. E. Dimotakis, “Measurements of scalar power spectra in high Schmidt number turbulent jets,” *J. Fluid Mech.* **308**, 129 (1996).

<sup>17</sup>B. S. Williams, D. Marteau, and J. P. Gollub, “Mixing of a passive scalar in magnetically forced two-dimensional turbulence,” *Phys. Fluids* **9**, 2061 (1997).

<sup>18</sup>D. C. Leslie, *Developments in the Theory of Turbulence* (Oxford University Press, Oxford, 1973).

<sup>19</sup>P. G. Saffman, “On the fine-scale structure of vector fields convected by a turbulent fluid,” *J. Fluid Mech.* **16**, 545 (1963).

<sup>20</sup>R. H. Kraichnan, “Small-scale structure of a scalar field convected by turbulence,” *Phys. Fluids* **11**, 945 (1968).

<sup>21</sup>G. R. Newman and J. R. Herring, “A test field study of a passive scalar in isotropic turbulence,” *J. Fluid Mech.* **94**, 163 (1979).

<sup>22</sup>T. S. Lundgren, “Turbulent pair dispersion and scalar diffusion,” *J. Fluid Mech.* **111**, 27 (1981).

<sup>23</sup>J. Qian, “Viscous range of turbulent scalar of large Prandtl number,” *Fluid Dyn. Res.* **15**, 103 (1995).

<sup>24</sup>C. W. van Atta, “Influence of fluctuations in dissipation rates on some statistical properties of turbulent scalar fields,” *Izv., Acad. Sci., USSR, Atmos. Oceanic Phys.* **10**, 712 (1974).

<sup>25</sup>R. H. Kraichnan, “Dispersion of particle pairs in homogeneous turbulence,” *Phys. Fluids* **9**, 1937 (1966).

<sup>26</sup>U. Frisch, A. Mazzino, A. Noullez, and M. Vergassola, “Lagrangian method for multiple correlations in passive scalar advection,” *Phys. Fluids* **11**, 2178 (1999).

<sup>27</sup>G. Falkovich, K. Gawedzki, and M. Vergassola, “Particles and fields in fluid turbulence,” *Rev. Mod. Phys.* **73**, 913 (2001).

<sup>28</sup>P. A. Durbin, “A stochastic model of two-particle dispersion and concentration fluctuations in homogeneous turbulence,” *J. Fluid Mech.* **100**, 279 (1981).

<sup>29</sup>D. J. Thomson, “A stochastic model for the motion of particle pairs in isotropic high-Reynolds-number turbulence, and its application to the problem of concentration variance,” *J. Fluid Mech.* **210**, 113 (1990).

<sup>30</sup>P. K. Yeung, “Correlation and conditional statistics in differential diffusion: scalars with uniform mean gradients,” *Phys. Fluids* **10**, 2621 (1998).

<sup>31</sup>Z. Warhaft, “Passive scalars in turbulent flows,” *Annu. Rev. Fluid Mech.* **32**, 203 (2000).

<sup>32</sup>A. M. Obukhov, “Structure of the temperature field in turbulent flows,” *Izv. Akad. Nauk SSSR, Ser. Geogr. Geofiz.* **13**, 58 (1949).

<sup>33</sup>S. Corrsin, “On the spectrum of isotropic temperature fluctuations in isotropic turbulence,” *J. Appl. Phys.* **22**, 469 (1951).

<sup>34</sup>A. S. Monin and A. M. Yaglom, *Statistical Fluid Mechanics: Mechanics of Turbulence* (MIT, Cambridge, MA, 1975), Vol. 2.

<sup>35</sup>M. Lesieur, *Turbulence in Fluids* (Kluwer, Dordrecht, 1997).

<sup>36</sup>M. F. Hibberd and B. L. Sawford, “Design criteria for water tank models of dispersion in the planetary boundary layer,” *Boundary-Layer Meteorol.* **67**, 97 (1994).

<sup>37</sup>B. L. Sawford, “Turbulent relative dispersion,” *Annu. Rev. Fluid Mech.* **33**, 289 (2001).

<sup>38</sup>S. B. Pope, “The vanishing effect of molecular diffusivity on turbulent dispersion: implications for turbulent mixing and the scalar flux,” *J. Fluid Mech.* **359**, 299 (1998).

<sup>39</sup>C. W. Gardiner, *Handbook of Stochastic Methods for Physics Chemistry and the Natural Sciences* (Springer, Berlin, 1983).

<sup>40</sup>P. G. Saffman, “On the effect of the molecular diffusivity in turbulent diffusion,” *J. Fluid Mech.* **8**, 273 (1960).

<sup>41</sup>R. H. Kraichnan, “Convection of a passive scalar by a quasi-uniform

- random straining field," *J. Fluid Mech.* **64**, 737 (1974).
- <sup>42</sup>W. Feller, *An Introduction to Probability Theory and Its Applications*, 2nd ed. (Wiley, New York, 1971), Vol. 2.
- <sup>43</sup>E. Balkovsky and E. Fouxon, "Universal long-time properties of Lagrangian statistics in the Batchelor regime and their application to the passive scalar problem," *Phys. Rev. E* **60**, 4164 (1999).
- <sup>44</sup>J. L. Lumley, "Some comments on turbulence," *Phys. Fluids A* **4**, 203 (1992).
- <sup>45</sup>M. R. Overholt and S. B. Pope, "Direct numerical simulation of a passive scalar with imposed mean gradient in isotropic turbulence," *Phys. Fluids* **8**, 3128 (1996).
- <sup>46</sup>K. R. Sreenivasan, "The passive scalar spectrum and the Obukhov-Corrsin constant," *Phys. Fluids* **8**, 189 (1996).
- <sup>47</sup>P. K. Yeung and B. L. Sawford, "Random-sweeping hypothesis for passive scalars in isotropic turbulence," *J. Fluid Mech.* **458**, 129 (2002).